Abstract for the 31st AIAA Applied Aerodynamics Conference,
San Diego, CA, June, 2013

Computational Assessment of the Benefits of Boundary Layer Ingestion for the D8 Aircraft

Shishir A. Pandya*
NASA Ames Research Center, Moffett Field, CA, USA
Alejandra Uranga
Massachusettes Institute of Technology, Cambridge, MA, USA

Abstract: To substantially reduce the fuel burn of future commercial transportation aircraft, the boundary layer ingestion idea is investigated. The idea is that an engine placed in the wake of the aircraft it is propelling is more efficient than a conventional engine placement under the wing or on pods mounted to the rear of the fuselage. The top, rear of the fuselage is thus designed to act as a diffuser such that the engines can be placed there with a minimal nacelle. The boundary layer thickens over the rear of the fuselage such that a large portion of it is ingested by the fan. To assess whether the boundary layer ingesting (BLI) engine placement is indeed advantageous, a study of the nacelle aerodynamics is carried out using Overflow, a viscous CFD flow solver that uses overset meshes. The computed forces and moments are compared to a wind tunnel experiment for validation. Some aspects of the design are verified using the simulation results. Finally, the effect of the nacelle placement is assessed by comparing the BLI nacelle configuration to a podded nacelle configuration and to the unpowered (without nacelles) aircraft.

Keywords: Overset, Aerodynamics, BLI, boundary-layer ingesting engine, D8, Double-bubble aircraft.

1 Introduction

The Fixed Wing (FW) Project in NASA's Fundamental Aeronautics program is developing technologies and concepts to drastically improve the energy efficiency and environmental impact of a future commercial transport aircraft. The project focuses on the 'N+3' timeframe (i.e. three generations beyond the current) with notional entry into service in approximately 2030-35. The project is leveraging both in-house and external expertise. The goal of the FW 'N+3' solicitation was to stimulate thinking to address future issues, such as reducing energy consumption, environmental

Figure 1: The MIT D8 "double-bubble" concept aircraft.

impact, noise, as well as dealing with future operations challenges. To achieve this, the program is identifying advanced airframe and propulsion systems concepts, and is working to bring enabling technologies to maturity.

---

*Aerospace Engineer, AIAA Senior Member

This paper presents a study of the boundary layer ingesting (BLI) nacelle design on the aerodynamics of an aircraft proposed by a team led by the Massachusetts Institute of Technology (MIT) called the D8 (double-bubble). The D8 aircraft incorporates enabling technologies in response to the NASA 'N+3' solicitation. With potentially major performance benefits, the D8 aircraft design [1, 2] is proposed as a Boeing 737 class aircraft that carries 180 passengers with a range of 3000 nmi (see Fig. 1). It is shorter than the 737-800 with a longer wingspan. The cruise speed of the D8 will be $M = 0.72$ which is lower than the 737's $M = 0.8$. The lower Mach number combined with a fuselage design that acts as a diffuser in the rear results in the flow reaching the engine fan face at approximately $M = 0.6$. A thick boundary layer that develops ahead of the fan face is ingested by the fan. It was proposed in [3] that similar to marine propulsion, there should be a large propulsion efficiency benefit from placing the fan in the wake or boundary layer of the vehicle so long as the fan is able to operate with non-uniform inflow.

Several benefits result from this design. First, since most engine fans are designed for $M = 0.6$, the proposed design minimizes the need for a large-inlet nacelle. The smaller nacelle means lower weight. Additionally, the fuselage can also be contoured to act as the lower part of the nacelle, further reducing weight. The empennage also contributes to weight reduction because the vertical pieces of the π-shaped tail can be used as the sides of the nacelle. This embedding of the engines into the rear of the fuselage and π-tail leads to a reduction in nacelle size and thus a reduction in nacelle drag as compared to a podded or under-wing nacelle.
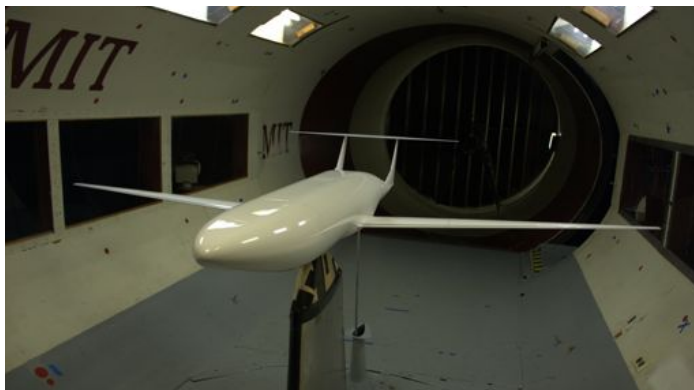

Figure 2: A photograph of the model in the MIT Wright brothers wind tunnel. (MIT)

Other advantages of the design, such as increased lift generated by the fuselage and a positive pitching moment at cruise condition resulting in a smaller wing and horizontal tail, were investigated in a previous paper [4]. These advantages, combined with other proposed design features such as advanced materials, and high bypass ratio small core engines, result in a highly efficient aircraft that meets the challenging performance metrics of NASA's FW Project.

A Computaiotnal Fluid Dynamics (CFD) study of the external aerodynamics characteristics of the aircraft without nacelles was presented in [4], along with validation against an experiment done in the Wright Brothers Wind Tunnel (WBWT) on a 1:20 scale model. The present paper applies the computational methodology developed in that previous study to evaluate the effect of the BLI nacelle design using CFD simulations of the entire aircraft with the BLI nacelles. To assess the benefit of the BLI, the results are compared to a podded nacelle configuration and the aircraft without nacelles. To validate the methodology, the results will be compared to additional wind tunnel (WT) data obtained by MIT on a 1:11 scale model of the D8 aircraft (Wind tunnel tests scheduled for Dec. 2012-Feb. 2013) with podded and embedded nacelles. Viscous computations are carried out using the structured overset mesh method at both WT conditions and flight conditions. The numerical modeling and solution methods are presented, followed by a discussion of the effects of various parts of the wind tunnel test model on the aerodynamics. A baseline mesh is created based on findings in previous investigations and the sensitivity of the solution on the mesh parameters is briefly discussed. Validation results are presented using the baseline mesh. A few of the design assumptions behind the D8 aircraft presented in [1, 2] and its preliminary performance estimates are assessed. Finally, an evaluation of the aerodynamics on the BLI nacelle design is presented.
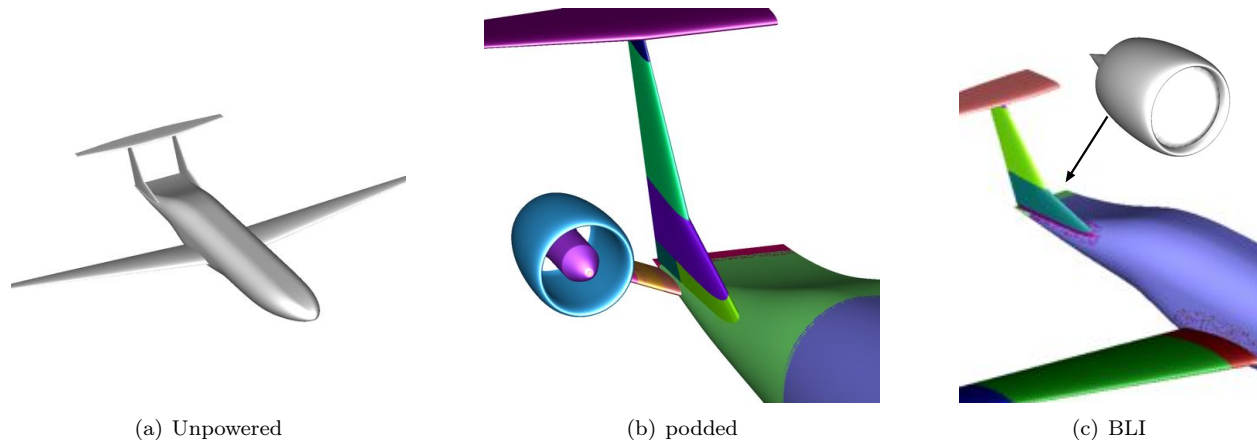
(a) Unpowered   (b) podded   (c) BLI

Figure 3: Various configurations of the D8 aircraft.

2 The D8 Configurations and Geometry

2.1 Model Configurations

Computations are performed on three versions of the D8 design to explore various aspects of the design's performance. These configurations are depicted in Fig. 3. The simplest configuration is comprised of the fuselage, wing, and empennage and is referred to as the unpowered configuration. The unpowered configuration has been used in previous studies to validate the methodology and will be used again here for further validation studies. Two outboard nacelles and hubs are mounted on the side of the fuselage in the rear (akin to a business jet or the MD-80 aircraft) to attain the podded configuration. This configuration will establish a baseline test case for an engine that only sees free-stream, undisturbed flow. Finally, the nacelle will be embedded into the rear, top of the fuselage to obtain the BLI nacelle configuration.

Two sources of reference geometry were employed. First, a set of structured patches with fine spacing that define the fuselage, wing, and empennage geometry were used to generate the meshes on those components. Second, the nacelle and a CAD model of the blended configuration was used to obtain meshes for the podded and blended configurations. In all cases, the x-axis is the stream-wise coordinate, y is the span-wise coordinate along the right wing and z is pointed upwards.

2.2 Wind Tunnel Configuration

A 1:11 scale model of the D8 aircraft was slightly modified for low-speed conditions and will be tested in the Wright Brothers Wind Tunnel (WBWT) at MIT at 120 mph (see Fig. 2) with the wings clipped so the model fits in the tunnel. The tests will be performed at various angles of attack. Boundary layer trips will be employed to assure turbulent flow on the wing, fuselage, and tail surfaces.

The tests will be conducted using the unpowered, podded, and BLI nacelle configurations. These tests will determine the aerodynamics effects of the nacelle placement and configuration.

In the final paper, simulations with the podded and blended nacelles will be included and will be compared to the 1:11 scale WBWT tests.

2.3 Modeling Wind Tunnel Walls and Mounting Hardware

It has been shown (See Figs. 4) that the WT walls and mounting hardware have an effect on the lift force even when the assumption of inviscid wind tunnel walls is adequate [4]. In contrast to that result for the 1:20 scale model, the 1:11 scale model is too large to fit inside the WBWT, so the tests will be done with the wings clipped. The edge of the clipped wings are close to the wind tunnel walls and thus a portion of the

wings will be in the boundary layer on the WT walls. Thus, it is important to model the wind tunnel walls accurately with viscous modeling. A detailed, viscous wall effects study on the 1:11 model will be reported in the final paper.
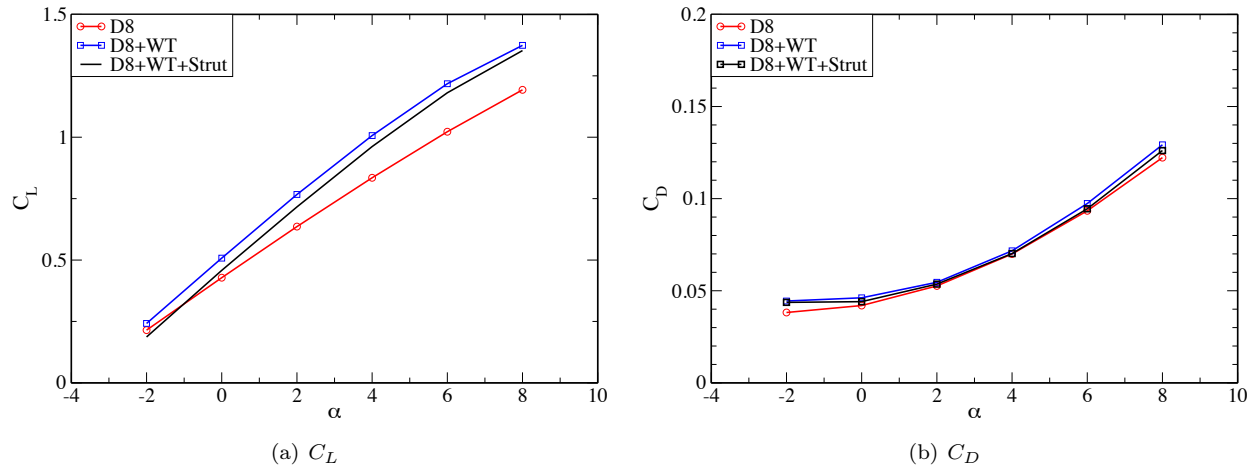

(a) C_L

(b) C_D

Figure 4: Comparison of lift and drag force coefficients as a function of the angle of attack with and without wind tunnel walls and mounting hardware from inviscid simulations.

To prepare for these tests and to guide the WT test matrix, CFD simulations are performed at 120 mph (approximately $M = 0.16$) for angles of attack between -2 and 14 degrees in 2 degree increments. All data are non-dimensionalized by the mean chord and wing surface area to provide the basis for consistent comparisons of forces. The geometry includes wind tunnel walls and the mounting hardware in the wind tunnel (see Fig. 5). Due to symmetry considerations, only the right half of the airplane and wind tunnel is modeled in all CFD simulations, thus lowering the number of grid points required and halving the computational cost. Care is taken to represent the geometry as closely as possible with the exception that no attempt is made to model small pieces of hardware such as the load balance rod between the mounting strut and the trunnion that supports the D8 model.

3 CFD Methodology

Structured overset mesh technology [5] is used to perform viscous simulations for the D8 configuration. The Chimera Grid Tools (CGT) package [6] is used to generate surface and volume meshes and the Overflow code [7] is used to obtain viscous solutions on the resulting meshes.

The viscous simulation process begins with either a reference surface triangulation or a reference panel network that defines the surface of the body. These reference surfaces can be derived from CAD or analytical means. Various CGT tools are accessed through the scripting library [8] to generate an overset structured surface mesh on each component of the aircraft. Collar grids are generated to discretize the volume around intersections between components (e.g. wing-fuselage junction). These overset surface meshes constitute the inputs to the volume mesh generation process. A hyperbolic mesh

Figure 5: A photograph of the mounting hardware in the MIT Wright Brothers wind tunnel. (MIT)

generation code in CGT [9] is used to generate the near-body volume meshes for the components of the D8

as well as for the WT walls and the mounting strut. To cover the space between the near-body grids and the WT wall grid, a set of Cartesian box grids are generated. Finally, the volumes up- and down-stream of the test section are covered with a core grid that follows the shape of the outer shell of the WT grid. Each step of the mesh generation process follows the overset mesh generation best practices [10] to decide the size of the grid cells and the amount of overlap between two overlapping grids.

Additionally, a set of solution adaptive meshes generated with the Aero module of the Cart3D code [11] was used on the unpowered D8 (without nacelles or pylons) to guide the decisions of where to cluster the overset meshes [4]. A typical adapted Cartesian mesh is shown in Fig. 6. The fact that the inviscid adjoint process results in a substantial amount of refinement in the fuselage/empennage interaction region means that a finer box grid is needed to cover that part of the volume. Furthermore, the additional refinement in the wing wake prompted the use of a specialized wake grid to capture the flow (shown in Fig. 7(a)). The wake grid overlaps the wing grid up to the trailing edge. It extends from the trailing edge to several chord lengths behind the wing. The wake grid has fine spacing at the trailing edge in all directions, but follows the

Figure 6: An automatically refined Cartesian embedded mesh for the D8 inviscid runs.

same spacing as the wing mesh in the span-wise direction. In the normal direction, the spacing is determined based on the viscous spacing needed to capture the wake. The spacing remains at that value for some distance above and below the trailing edge, and stretches after that. The mesh also stretches in the downstream direction. This type of mesh is able to properly cluster points in the wake region, which is an advantage over the standard o-mesh topology. An additional benefit of this specialized mesh is that one can cluster the mesh near the wing tip to capture the tip vortex in more detail. The resulting tip vortex is shown in Figs. 7(b) and (c).
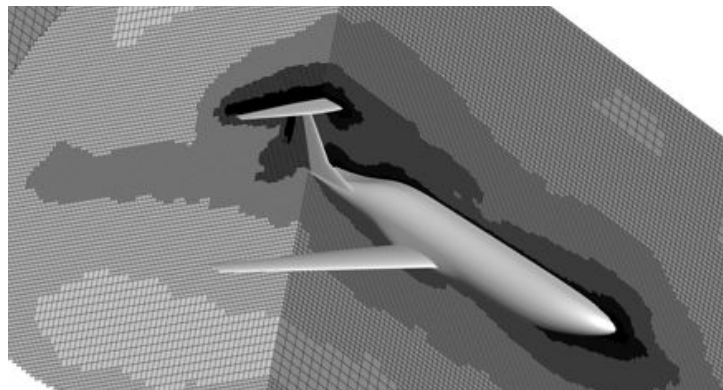
The resulting mesh is fed into the Overflow code, along with initial and boundary conditions to obtain viscous solutions for the D8 aerodynamics with and without the nacelles and hub. The internal X-rays module [12] of the Overflow code is used to obtain mesh connectivity and interpolation coefficients to facilitate communication between two overlapping grids.

Using the overset best practices and the preliminary guidance from the Cart3D adapted mesh, a baseline mesh was developed. This mesh is created with a uniform layer of cells next to the body with a target y^+ of 1. Several meshing parameters are used to characterize the grid generation process. The growth of the near-wall spacing in the wall-normal direction is referred to as stretching ratio and has a nominal values of 1.15. The spacing in the off-body uniform Cartesian box grids is set to approximately 5% of the mean
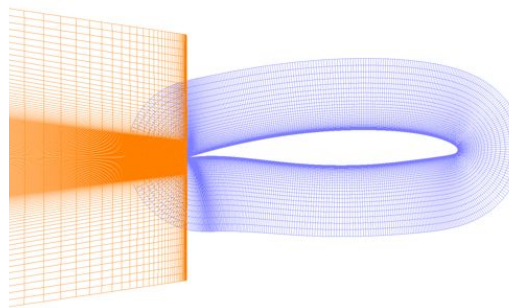
(a) 2D slice of a wing and wake grid.
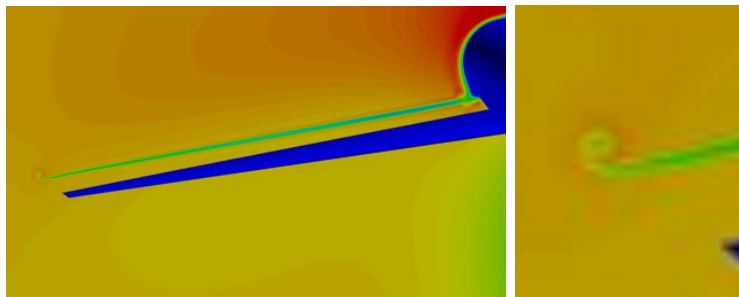
(b) Planar cut behind the wing showing the tip vortex.

(c) Zoom-in view of the tip vortex.

Figure 7: A specialized mesh for capturing the wake and tip vortex.
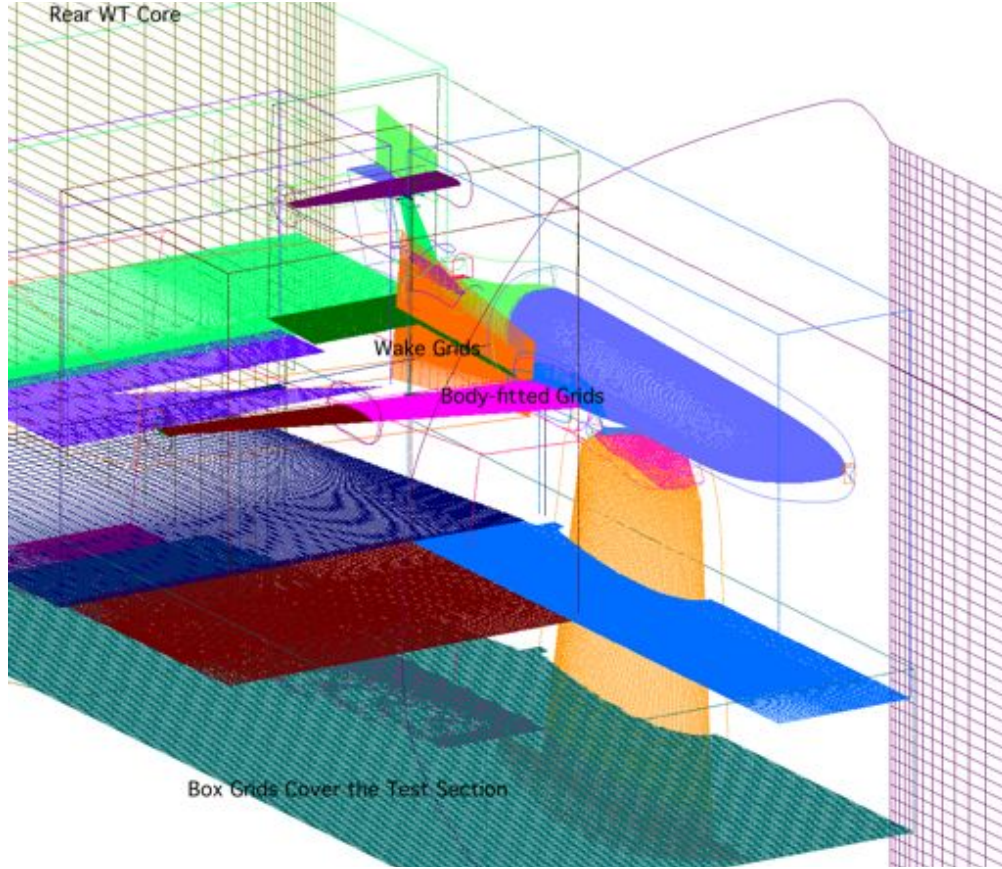
Figure 8: The anatomy of the overset mesh used for the Overflow viscous simulations.

chord. A characteristic surface spacing parameter is defined to be 1 when the leading edge spacing is 0.1% of the mean chord. The trailing edge spacing is generally set to half of the leading edge spacing. These choices result in a surface mesh which has approximately 550 points defining the root airfoil and 300 points defining the tip airfoil with the mesh stretching to coarser spacing in flatter regions compared to the leading and trailing edges. The resulting baseline mesh, shown in Fig. 8, is 35 overset volume meshes containing approximately 80 million points for the D8, WT walls, and mounting strut. The nacelles and hub add another 4 to 9 million points to the mesh.

Several consistency checks were performed to assure that the solution methodology is accurate in [4]. A comparison of various solution methods, time-accurate , boundary conditions, low-Mach preconditioning, and hole-cutting methods reveals that the Beam-Warming approximate-factorization scheme [13] is the most robust with minimal variation in the integrated forces. As a result of these consistency comparisons, all computations performed with the Overflow code in this study use the Beam-Warming approximate-factorization scheme with a central-differenced right hand side in steady mode without a low-Mach number pre-conditioner. In the final paper, the wind-tunnel walls for the 1:11 scale model will be treated with accurate WT wall geometry and will be modeled as viscous wall boundaries to account for boundary layer growth. The spatial accuracy of the central-differenced right-hand side is formally second order. The SST turbulence model[14] is chosen based on a study done in [4]. A typical solution convergence of the resulting solution process is shown in Fig. 9. The L2-norm of the right-hand-side residual is plotted for all grids and it can be seen that all grids converge approximately 4 to 5 orders of magnitude. A typical solution on the unpowered configuration is shown in Figs. 10(a).
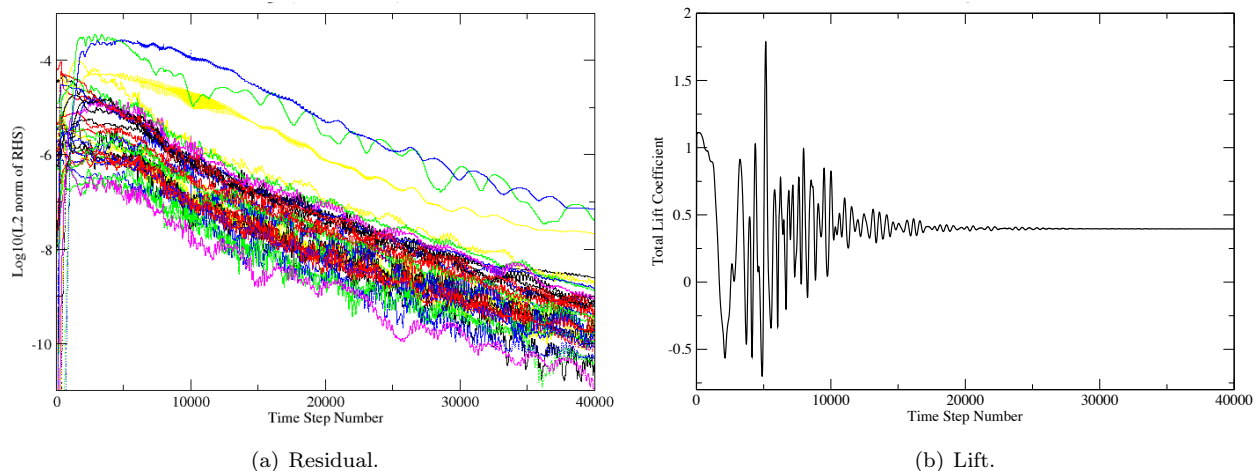
(a) Residual.

(b) Lift.

Figure 9: A typical convergence in Overflow.
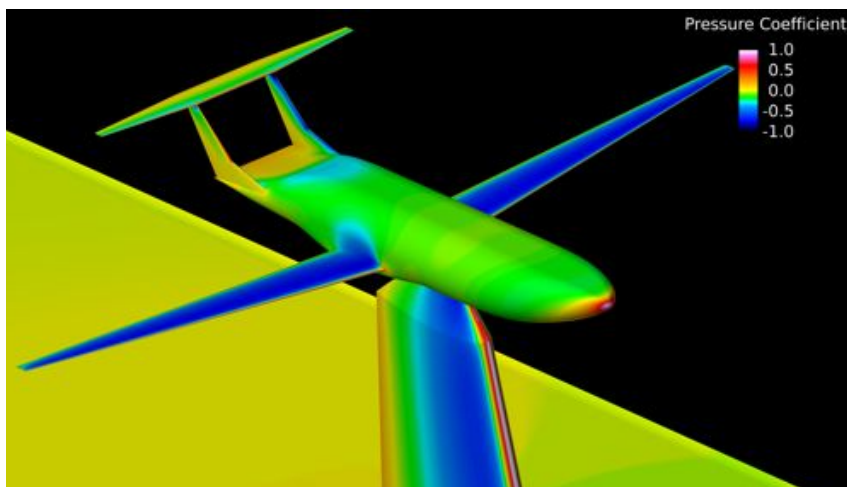

Figure 10: A typical Overflow solution on the unpowered D8 aircraft (pressure contours).

4   Solution Sensitivity to Mesh Parameters

A study of solution sensitivity to various meshing parameters was carried out in [4]. Four major parameters were tested independently, namely the wall spacing (target y^+), surface spacing (wing leading edge spacing, trailing edge spacing, and global spacing parameters on the surface), near-wall stretching ratio, and off-body spacing. The meshes for this study are generated using mesh parameters close to the baseline mesh. Based on this study, a y^+ of 1, a fine mesh reference value of 0.5, a stretching ratio of 1.15, and off-body spacing corresponding to 0.15 inches is used. Here, the surface spacing reference of 0.5 corresponds to a spacing of 0.1 inches (1.6% of chord) in the middle of the top and bottom surfaces of the wing. The leading edge is 0.006 inches (0.1% of chord), and the trailing edge spacing is half of the leading edge spacing. All other surfaces (e.g. fuselage, π-tail) follow similar surface mesh spacing rules and are a function of the same reference value.

A similar study on the podded and blended configurations will be carried out to assure proper independence from changes in meshing parameters.
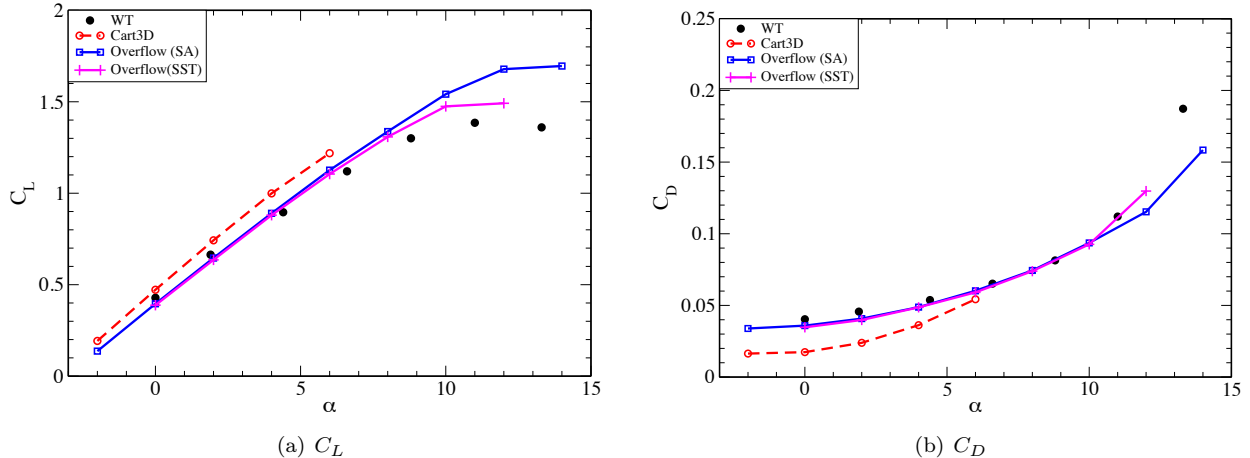
Figure 11: Comparison of lift and drag coefficients (Cart3D inviscid CFD, Overflow viscous CFD and MIT wind tunnel experiment). The vehicle is modeled with wind tunnel walls and mounting hardware.

5   Validation

The computational results from viscous simulations are presented and compared to inviscid Cart3D [11] results and the MIT wind tunnel experiment at $M = 0.16$ for angles of attack between -2 and 14 degrees for the 1:20 model. The integrated lift and drag coefficients are compared to the wind tunnel results and the trends are discussed. In the final paper, the 1:11 scale model results and comparison to a WT test will be shown.

Figure 11(a) shows the lift coefficient as a function of angle of attack. The lift coefficients from the Cart3D and Overflow results compare well to the experimental results with Cart3D predicting slightly higher lift than the wind tunnel values at low angles of attack and Overflow resulting in a higher lift at high angles of attack. The steady Cart3D simulations become oscillatory above an angle of attack of $6°$. This makes it difficult to converge to a value, thus the lift coefficient values from Cart3D are not reported above this α. Both Spalart-Allmaras and Menter-SST turbulence model results are presented. Both models predict the lift at lower angles of attack with reasonable accuracy, but SST predicts more separation on the top of the wing, normally associated with stall. Thus, SST appears to be more accurate at higher α values.

The drag comparison for the same α sweep is shown in Fig. 11(b). The drag prediction from Cart3D is lower than the WT data and the Overflow results owing to the fact that it does not include the viscous drag. Once again, the Cart3D solutions at higher angles of attack are not reported. The Overflow results are very close to the WT data with the SST turbulence model matching the experiment better at $\alpha = 12°$. $\alpha = 14°$ was not calculated with SST due to difficulties in obtaining a solution. Due to the better agreement with WT data at higher angles of attack, the Menter-SST turbulence model will be used in all calculations for this paper.

6   Results

The final paper will include various results and comparisons in order to draw conclusions regarding the expected benefits of BLI. Simulation results for the aircraft at cruise conditions will be shown and will be compared to the podded and embedded configurations to highlight the effects of the nacelle placement.

An example simulation result on a podded configuration aircraft is discussed below. Figure 12 shows pressure contours on a typical podded configuration. The final paper will include solutions on podded and BLI configurations. Comparisons of the lift and drag for α sweeps of the unpowered and podded configurations will be made to the BLI configuration. It will also attempt to draw conclusions about the effects of placing the nacelles in the boundary layer by contrasting the BLI configuration results with the podded configuration. Finally, we will examine the proposed advantages of the D8 aircraft to assure that the D8 with BLI nacelles indeed provides the advantages expected by Drela [1].

The final paper will also include a comparison of the podded and embedded configurations in order to draw conclusions that will help determine if the expected benefits of BLI do indeed exist. We will also explore various aspects of the D8 design such as the lift, drag, and $\frac{L}{D}$ to detail the effects of BLI on those parameters.
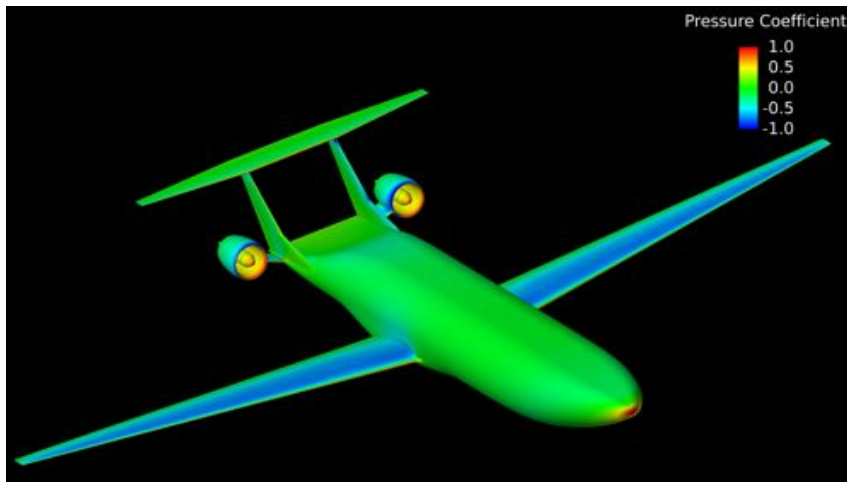

Figure 12: Pressure contours on a podded D8 aircraft.

7 Summary and Concluding Remarks

The effect of boundary layer ingesting nacelles will be studied using a viscous computational study for three separate configurations of the D8 aircraft. Overset mesh technology is used to obtain the meshes for the various configurations. The mesh generation process followed studies done on the external aerodynamics of the D8 aircraft to assure proper mesh density and quality. Adjoint-based mesh refinement is used with inviscid simulations at low angles of attack to guide some aspects of the viscous mesh generation process. A baseline viscous mesh is used to obtain an alpha sweep on the D8 in the wind tunnel with mounting strut at $M = 0.16$. The results are validated against the Wright Brothers Wind Tunnel test data for the 1:20 scale model and the final paper will contain similar studies for the 1:11 model. It is found that the SST turbulence model predicts lift and drag values that are closer to the WT data. The final paper will present results for the embedded nacelles and the aircraft performance will be compared to that of the podded nacelle configuration.

Acknowledgements

References

[1] M. Drela. Development of the D8 Transport Configuration. AIAA Paper 2011–3970, 2011.

[2] E. M. Greitzer et. al. N+3 Aircraft Concepts Designs and Trade Studies, Final Report. NASA CR 2010-216794, 2010.

[3] L. H. Smith Jr. Wake Ingestion Propulsion Benefit. *Journal of Propulsion and Power*, 9(1):74–82, 1993.

[4] S. A. Pandya. External Aerodynamics Simulations for the MIT D8 ÒDouble-BubbleÓ Aircraft Design. ICCFD7-4304, 2012.

[5] W. M. Chan. Overset Grid Technology Development at NASA Ames Research Center. *Computers & Fluids*, 38:496–503, 2009.

[6] William M. Chan. Developments in Strategies and Software Tools for Overset Structured Grid Generation and Connectivity. AIAA-2011-3051, 2011.

[7] P. G. Buning, D. C. Jespersen, T. H. Pulliam, G. H. Klopfer, W. M. Chan, J. P. Slotnick, S. E. Krist, and K. J. Renze. OVERFLOW User's Manual. NASA, 2005.

[8] S. A. Pandya and W. M. Chan. Automation of Structured Overset Mesh Generation for Rocket Geometries. AIAA Paper 2009–3993, 2009.

[9] W. M. Chan and J. L. Steger. Enhancements of a Three-Dimensional Hyperbolic Grid Generation Scheme. *Appl. Math & Comp.*, 51:181–205, 1992.

[10] W. M. Chan, R. J. Gomez, S. E. Rogers, and P. G. Buning. Best Practices In Overset Grid Generation. AIAA Paper 2002-3191, 2002.

[11] M. Nemec and M J. Aftosmis. Adjoint-Based Adaptive Mesh Refinement for Complex Geometries. AIAA Paper 2008–0725, 2008.

[12] R. L. Meakin. Object X-rays for Cutting Holes in Composite Overset Structured Grids. AIAA paper 2001–2537, 2001.

[13] R. M. Beam and R. F. Warming. An Implicit Factored Scheme for the Compressible Navier-Stokes Equations. *AIAA Journal*, 16(4):393–402, 1978.

[14] F. R. Menter. Two-Equation Eddy-Viscosity Turbulence Models for Engineering Applications. *AIAA Journal*, 32(8):1598–1605, 1994.